Optimization of Surface Modifications to Enhance Cryogenic Pool Boiling

Shuba Murthy

A thesis
submitted in partial fulfillment of the
requirements for the degree of

Master of Science in Aeronautics and Astronautics

University of Washington

2025

Reading Committee:
James Hermanson, Chair
Carl Knowlen

Program Authorized to Offer Degree:
Aeronautics & Astronautics

University of Washington

Abstract

Optimization of Surface Modifications to Enhance Cryogenic Pool Boiling

Shuba Murthy

Chair of the Supervisory Committee:
Professor James Hermanson
Aeronautics & Astronautics

Cryogenic boiling plays a pivotal role in propulsion and thermal management systems, where efficient heat transfer is essential. Enhancing nucleate boiling through surface modifications has emerged as a promising passive technique to improve heat flux. Building on prior work, which demonstrated improved performance using axially grooved aluminum cylinders, this study investigates the effects of two additional surface treatments: a wider 3 mm groove spacing and a knurled pattern with a 10° pitch angle and 0.03 mm depth.

Heat flux was estimated from thermocouple-based temperature profiles using a one-dimensional conduction model, independent of electrical input power. Results show a distinct performance hierarchy influenced by surface geometry: the 2 mm grooved surface delivered the highest heat flux, followed by the 3 mm grooved and knurled surfaces, which showed reduced performance due to lower nucleation site density and altered wetting dynamics. These findings highlight the sensitivity of cryogenic boiling to fine-scale surface geometry and support ongoing development of optimized surface designs for advanced cryogenic systems. We developed an imaging protocol using an externally purged endoscope to visualize nucleate boiling in LN_2; preliminary images on a 2.5 cm OD cylinder indicate characteristic bubble diameters of $\sim$2 mm, while frame-rate limits precluded departure-velocity estimates. A custom two-viewport cryogenic dewar (with planned Phantom high-speed camera) will enable quantitative bubble-dynamics measurements.

TABLE OF CONTENTS

LIST OF FIGURES

NOMENCLATURE

A	=	Surface area of smooth cylinder (m^2)
A_g	=	Surface area of grooved cylinder (m^2)
g	=	Gravitational acceleration (m/s^2)
h	=	Convective heat transfer coefficient, smooth ($W/m^2 \cdot K$)
h_g	=	Heat transfer coefficient, grooved area-corrected ($W/m^2 \cdot K$)
h_f	=	Heat transfer coefficient, fin-effectiveness-corrected ($W/m^2 \cdot K$)
k	=	Thermal conductivity of cylinder ($W/m \cdot K$)
L	=	Length of cylinder (m)
Q	=	Heat flow (W)
q	=	Heat flux (W/m^2)
R_t	=	Total radial thermal resistance (K/W)
r	=	Radial position in cylinder (m)
r_b	=	Radius at base of fin (m)
r_i	=	Inner radius of cylinder (m)
r_o	=	Outer (surface) radius of cylinder (m)
r_{crit}	=	Critical bubble radius (m)
T	=	Temperature in cylinder as a function of radius (K)
T_i	=	Inner (heater-side) temperature of cylinder (K)
T_{sur}	=	Surface temperature of cylinder (K)
T_∞	=	Ambient bath temperature (K)
t_b	=	Thickness of space between fins (m)

t_f	=	Thickness of fin (m)
ρ_l	=	Density of liquid (kg/m^3)
σ	=	Surface tension (N/m)

List of Subscripts

g	=	Grooved cylinder
f	=	Fin correction
b	=	Fin base
i	=	Inner cylinder location
o	=	Outer cylinder location
sur	=	Surface
∞	=	Ambient bath (LN_{22} at 77.34 K)

ACKNOWLEDGMENTS

I would like to sincerely thank Benjamin Dunh and Nathan Paradez for their skilled machining work and hands-on assistance throughout the project. I also thank Andrew Jansen and Andrew Jacob for their guidance and support. I am grateful to Professor Carl Knowlen and Professor Dabiri for their valuable input, and to Mr. Gary Grayson, Michael Friedman, and Scott Sherod for their collaboration and insight. This work was conducted jointly with Blue Origin and was supported by the Washington State JCATI program for 2024-2025. Most of all, I extend my deepest thanks to my thesis advisor, Professor Jim Hermanson, for his mentorship, patience, and endless support.

DEDICATION

To my dearest mother, Saveitha, and my father, Murthy — for their unwavering patience, support, and thoughtfulness.

To the little homie Adi, I hope I can make life easier for you someday and to Leo, for being the sweetest treat in our lives.

To Aman, Aditi, Navdha, Zahabiya, Barua, Surya, Dennis, Sharan, Jyothi, Mehak, Manjari, Meenal, Kaamakshee, Fatwir, Hemanth, Kaeli, Nithin, Thomas, Bennett, Isabella, Lauren, Mikhail, Hannah, Brenda, Auggie, Rocky, Conner, Hucky, Vaish, Sriram, Khushi, Punya, Krithika, Ankita, Achu anna, and Jeshu akka, among many others, for all the laughter, food, music and warmth that guided me. It is the greatest joy to learn from you. Thank you for being in my corner, I hope to be in yours too.

To spiders, bumblebees, moths, ladybugs, craneflies, butterflies, birds, beavers, squirrels, centipedes, and all the critters of the Pacific Northwest. I will never stop being amused by you.

Chapter 1
INTRODUCTION

1.1 Technical background and approach

Cryogenic liquids play a critical role in space systems. Liquid hydrogen and liquid oxygen are high-performance bipropellants for launch and propulsion, while liquid oxygen also provides breathable air for cabins and spacesuits[1]. Cryogenic hydrogen and oxygen can be converted to gaseous forms for fuel cells, supplying electrical power, and for Reaction Control System (RCS) thrusters. The autogenous generation of high-pressure gas from cryogenic boiling reduces or eliminates the reliance on hypergolic propellants, an important factor for reusable and long-duration space vehicles.

Beyond aerospace, cryogenic fluids are central to terrestrial technologies such as high-power electronic cooling and superconductivity[2]. These applications underscore a mission-critical need for efficient, compact, and lightweight cryogenic-fluid devices. Pool boiling, in particular, is central to cryogenic boiler systems under consideration for future spacecraft, including those by Blue Origin. The goal of this research is to identify and develop geometric and surface configurations that optimize pool-boiling effectiveness for cryogenic boiler applications.

1.2 Fundamentals of Pool boiling

Pool boiling is a highly effective method of transferring heat through vapor generation [3, 4]. As the wall temperature rises above saturation, bubbles first appear at active nucleation sites, marking the onset of nucleate boiling (ONB). With increasing heat input, vapor escapes more vigorously, producing a maximum heat flux known as the critical heat flux (CHF). Beyond CHF, film boiling occurs, where a vapor layer insulates the surface and drastically reduces heat transfer.

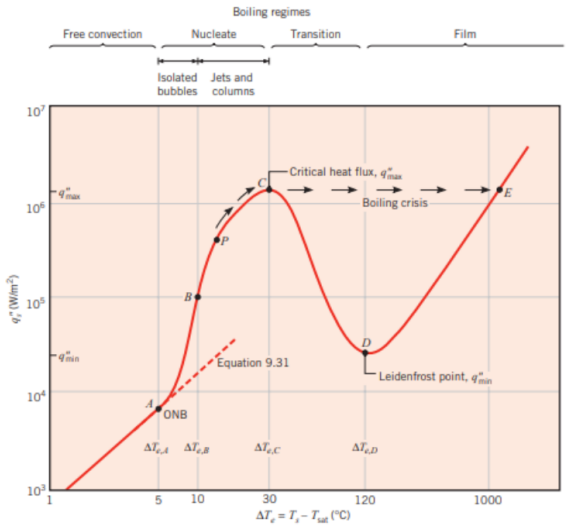

Figure 1.1: Typical boiling curve for water at 1 atm pressure

Bubble dynamics play a key role in this process. At low heat flux, small bubbles are isolated, while at higher flux they merge into clusters as CHF is approached. The number and distribution of nucleation sites are strongly dependent on surface temperature and geometry [5, 6]. Visualizations to date have generally been limited to smooth wall surfaces [7], highlighting a gap in understanding how engineered surface modifications alter boiling regimes in cryogenic fluids.

1.3 Previous Studies on Cryogenic Pool Boiling

Extensive work has been done to characterize pool boiling across a range of fluids, geometries, and operating conditions. These studies have led to empirical correlations [4] and theoretical models [6] that predict ONB, CHF, and the Leidenfrost Point (LFP). However, large discrepancies remain between reported results, with variations often exceeding an order of magnitude for similar configurations [8]. A significant portion of this uncertainty arises from experimental challenges in temperature measurement, heat flux calculation, and surface characterization.

Surface condition has been identified as one of the strongest influences on boiling performance. Reported surface modifications include porous coatings [9, 10], roughened or oxidized surfaces [11], grooves and channels [12], and micro/nano-structured surfaces [4]. These techniques generally increase nucleation site density, modify bubble departure size and frequency, and increase effective surface area. While many studies have demonstrated substantial enhancements in heat transfer, relatively few have focused on cryogenic fluids [11].

Preliminary work at the University of Washington has shown that even simple modifications, such as adding smooth grooves to a cylindrical surface, significantly improve the heat transfer rate in liquid nitrogen compared to a polished baseline [13]. These results suggest that combining multiple geometric approaches—such as porous coatings with grooves or fins—may further enhance performance, offering a promising path for cryogenic boiler optimization.

1.4 Objectives of this Study

The purpose of this research is to systematically investigate how surface geometry and condition influence pool boiling in cryogenic liquids, with liquid nitrogen (LN_2) serving as a non-reactive analog to liquid oxygen. Specific objectives include:

1. Characterize bubble dynamics — using high-speed imaging to quantify bubble departure rates, sizes, and nucleation-site densities.

2. Quantify heat transfer performance — comparing smooth, grooved, and fin-like surfaces under identical heating and diagnostic conditions.

3. Identify optimized surface geometries — correlating bubble dynamics with measured heat flux to determine which modifications yield the highest performance. Support spaceflight boiler design — providing experimental data and validated configurations to industry partners (Blue Origin) for future cryogenic boiler systems.

Through this work, a more complete understanding of cryogenic pool boiling will be developed, directly connecting bubble-scale dynamics with macroscopic heat-transfer performance. This connection is expected to yield surface configurations that provide reliable, lightweight, and efficient cryogenic boilers for long-duration space missions.

Chapter 2
EXPERIMENTAL APPARATUS AND DIAGNOSTICS

2.1 Overview and Working Fluid

Experiments in this study use liquid nitrogen (LN_2), a non-reactive cryogenic fluid for which there is a large, existing database of results [8], and which is thermodynamically very similar to liquid oxygen. All tests are conducted at atmospheric pressure with the test article immersed in a static bath. The experimental configuration consists of an insulated vessel of inner diameter 34.3 cm containing approximately 17 L of LN_2, fitted with a horizontal test specimen as shown in Figure 2.3. Heating is provided by embedded electrical cartridge heaters.

2.2 Heater Geometry and Test Articles

Pool boiling has been investigated in a variety of geometries (wires, plates, cylinders). Cylinders were selected here for their azimuthal symmetry, enabling dominant one-dimensional radial conduction for heat-flux estimation.

2.2.1 Dimensions and L/D Selection

To minimize end effects, the cylinder length-to-diameter ratio was chosen to be at least 10:1. The interior diameter $d_i = 0.64$ cm (to accommodate commercial cartridge heaters) and outer diameter $d_o = 2.5$ cm were selected. The overall length was $L = 26.5$ cm, yielding $L/d_o \approx 10.6{:}1$.

2.2.2 Surface Configurations

Three surface conditions were tested:

1. **Smooth (baseline):** Turned/polished aluminum cylinder.

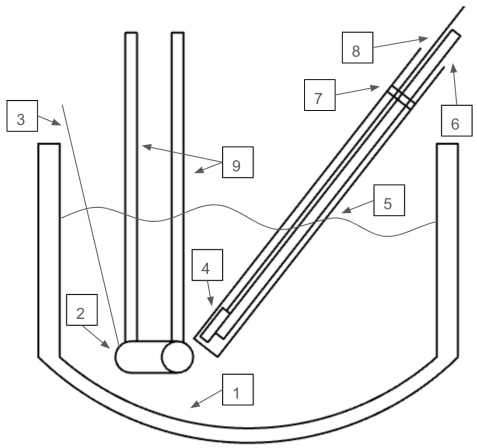

Figure 2.1: heater configuration (schematic). (1) insulated container; (2) test surface (horizontal); (3) cartridge heater; (4) submerged action camera (waterproof housing); (5) mounting rods; (6) Helium input; (7) Plug support; (8) Boroscope wire; (9) Mounting rods

2. **Axially grooved:** Square, straight-wall grooves machined uniformly along the length. Two groove sets are referenced in this work:

   (a) The baseline set following specimens with groove width, depth, and spacing of 2 mm each

   (b) Follow-on set used to probe sensitivity featuring 3 mm spacing with groove depth 2 mm and ridge height 2 mm (a 1 mm change from the baseline spacing).

3. **Knurled:** A crosshatched roughened surface produced using the coarsest available knurling tool (pitch angle 10°, depth ≈ 0.029 in or 0.74 mm) on an aluminum cylinder with the same outer diameter as the grooved specimens (worked length ≈ 10 in).

All grooved samples were machined so that the grooves are interior to the nominal outer diameter; therefore, all cylinders share the same $d_o = 2.5$ cm. The outer thermocouple on grooved cylinders is situated at the base of a fin (see Figure 2.4)

(a) Grooved 3 mm cylinder

(b) Knurled surface

Figure 2.2: Test articles shown side by side: grooved (left) and knurled (right).

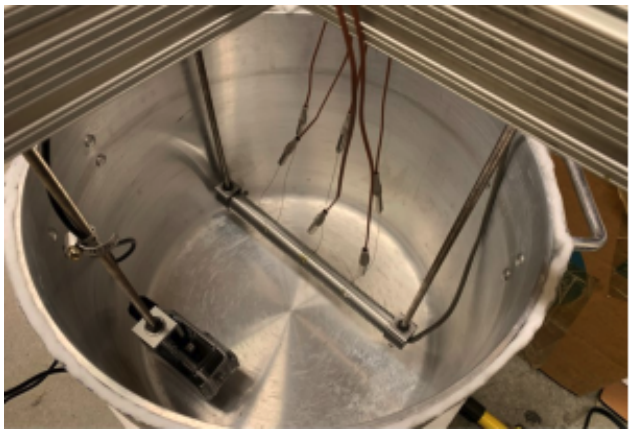

Figure 2.3: Horizontally mounted grooved cylinder.

2.3 Test Chamber and Mounting

The insulated vessel (dewar) is instrumented to allow either horizontal or vertical mounting of the cylinder (Fig. **??**). Optical access for visualization is provided with a submerged action camera in a waterproof housing, powered externally. Mounting rods allow repeatable placement. Vent/fill lines, electrical feedthroughs, and thermocouple leads are routed to minimize flow disturbance near the test article.

2.4 Diagnostics and Instrumentation

2.4.1 Thermometry and Heat-Flux Sensing

Multiple copper–constantan (Type T) thermocouples are embedded at prescribed radial locations to measure inner and outer wall temperatures. On grooved cylinders, the outer thermocouple well is positioned at the fin base; on smooth cylinders, it is located at the nominal outer radius. Each thermocouple well is packed with Apiezon N thermal grease to exclude LN_2 and ensure good thermal contact. The stated thermocouple uncertainty is $\pm 0.3°C$.

2.4.2 Imaging and Illumination

Boiling visualization is performed with a submerged action camera (waterproof enclosure) connected to an external power supply. A xenon arc lamp provides high-intensity illumination to resolve bubble dynamics near the surface. Representative schematic configurations are shown in Figure 2.1.

2.5 Experimental Procedure

1. **Chamber fill and Cooldown:** The dewar is filled with LN_2 and allowed to cool to saturation conditions.

2. **Specimen insertion and sealing:** The test cylinder is slowly lowered into the LN_2 bath to allow the Apiezon N grease within thermocouple wells to harden and form a liquid-tight seal.

3. **Thermal equilibration:** The cylinder is allowed to equilibrate to the bath temperature.

4. **Heating step:** A specified electrical input power is applied to the embedded cartridge heater and maintained for 5 min to approach quasi-steady conditions.

5. **Cooldown step:** The heater is switched off; the specimen is allowed to cool for 4 min to return near the ambient LN_2 temperature.

6. **Incremental testing:** Steps 4–5 are repeated for a sequence of voltage (power) settings spanning the nucleate boiling regime and approaching CHF, as allowed by safe operation.

7. **Data averaging:** During each quasi-steady heating period, thermocouple readings are time-averaged to obtain representative inner and outer wall temperatures for heat-flux calculation.

2.6 Data Reduction

Heat transfer is evaluated by coupling measured wall temperatures with a 1D radial conduction model that accounts for the temperature dependence of the aluminum thermal conductivity $k(T)$ at cryogenic temperatures (NIST data [12]). The outer-surface heat flux is then paired with the extrapolated surface temperature to compute the convective heat transfer coefficient.

2.6.1 Governing Relations

The relevant equations are [13]:

$$Q \;=\; -\,k\,A\,\frac{dT}{dr} \;=\; h\,A\,(T_{\mathrm{sur}} - T_{\infty}), \tag{2.1}$$

$$T(r) \;=\; \frac{T_i - T_{\mathrm{sur}}}{\ln\!\left(\frac{r_i}{r_o}\right)}\,\ln\!\left(\frac{r}{r_o}\right) \;+\; T_{\mathrm{sur}}, \tag{2.2}$$

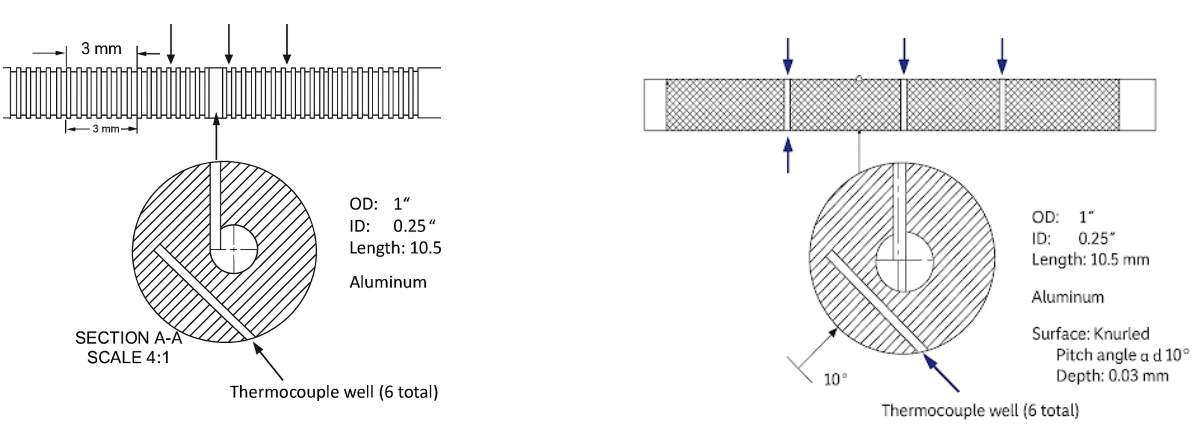

Figure 2.4: Grooved Cylinder Geometry (left) and Knurled Cylinder Geometry (right).

$$R_t \;=\; \sum_{n=1}^{N} \frac{\ln\!\left(\frac{r_{n+1}}{r_n}\right)}{2\pi L\, k_n}, \qquad N = 1000, \tag{2.3}$$

$$Q \;=\; \frac{T_i - T_{\text{sur}}}{R_t}. \tag{2.4}$$

Equation (2.1) expresses conservation of energy at the surface; Eq. (2.2) is the logarithmic temperature distribution for a hollow cylinder under steady 1D radial conduction; Eq. (2.3) computes the composite thermal resistance using N=1000 radial elements with $k_n \equiv k\!\left(\frac{T(r_n)+T(r_{n+1})}{2}\right)$ from NIST [12]; Eq. (2.4) gives total heat flow. The outer-surface heat flux q_o'' is obtained from Q and the outer area, and h follows from $q_o'' = h\,(T_{\text{sur}} - T_\infty)$.

2.6.2 Heater

Figure 2.4 shows cross-sections indicating inner and outer thermocouple well positions. On the grooved cylinder, the outer well is moved inward slightly to the fin base relative to the smooth cylinder. These locations are used as r_i and r_o in Eq. (2.2) and to construct the discretized r_n in Eq. (2.3).

2.6.3 Accounting for Variable Thermal Conductivity

To quantify the effect of variable $k(T)$, heat-flux profiles computed with temperature-dependent conductivity are compared against profiles obtained assuming constant k. Incorporating $k(T)$ produces an overall $\sim 2\%$ decrease in the estimated heat flux relative to the constant-k assumption under the present operating conditions.

2.7 Heat Flux Calculation and Validation

The heat flux in our cryogenic nucleate boiling experiments was estimated using a simplified conduction model based on Fourier's Law:

$$q = \frac{k \cdot A}{L} \cdot (T_{\text{wall}} - T_{\text{sat}}) \tag{2.5}$$

Where:

- q is the total heat transfer rate (W)
- $k = 0.3\,\text{W/m} \cdot \text{K}$ is the thermal conductivity of aluminum at cryogenic temperatures
- $A = 0.0006\,\text{m}^2$ is the surface area for heat transfer (assumed)
- $L = 0.003\,\text{m}$ is the wall thickness of the cylinder
- T_{wall} is the measured surface temperature (in K)
- $T_{\text{sat}} = 77.34\,\text{K}$ is the saturation temperature of LN_2 at 1 atm

Rewriting in terms of heat flux per unit area ($\dot{q}''$):

$$\dot{q}'' = \frac{q}{A} = \frac{k}{L} \cdot (T_{\text{wall}} - T_{\text{sat}}) \tag{2.6}$$

Substituting the constants:

$$\dot{q}'' = \frac{0.3}{0.003} \cdot (T_{\text{wall}} - 77.34) = 100 \cdot (T_{\text{wall}} - 77.34) \tag{2.7}$$

Validation and Discussion

The calculated values fall within the expected range for nucleate boiling in LN_2. Literature reports heat fluxes ranging from 500 to 5000 W/m^2 depending on surface condition, orientation, and subcooling.

Our dataset peaks around 2500–3000 W/m^2, which is:

- Consistent with nucleate boiling, especially on enhanced surfaces (e.g., grooved or knurled).
- Below the critical heat flux (CHF) of ∼10,000–20,000 W/m^2 for LN_2 on smooth surfaces.

This agreement indicates that the simplified conduction-based methodology provides physically valid and relevant estimates for cryogenic pool boiling performance.

2.8 Uncertainty Analysis

The stated thermocouple temperature uncertainty is ±0.3°C at each measurement location. Combined with uncertainties in thermocouple radial placement, groove geometry (for grooved/knurled specimens), and the temperature dependence and tabulation of $k(T)$, the overall uncertainty in the heat-flux estimate is approximately 20% for the present configuration and methodology. This aggregate value reflects error propagation through Eqs. (2.2)–(2.4) and sensitivity to $k(T)$ in the discretized resistance computation.

2.9 Notes on Groove/Knurl Selection

Groove spacing and cylinder material were selected for manufacturing simplicity and for the availability of NIST thermal conductivity data for aluminum at cryogenic temperatures [12]. The knurled texture was chosen to increase effective area and potential nucleation-site density while remaining compatible with the same heater geometry and outer diameter, enabling direct comparison to both smooth and grooved surfaces.

Chapter 3

RESULTS

The calculated theoretical temperature profile from Eq. 3 is shown in Fig. 3.1 (a). The corrected heat flux profile, shown in Fig. 3.1 (b), is derived from Eq. 5 after dividing by the area of the cylinder at a given radial location. Using the calculated heat flux value at the surface and the surface temperature, T_{sur}, the nucleate boiling curve can be plotted for different heater power inputs.

The observed differences between the smooth, grooved and knurled cylinders are shown in Fig. 3.2. the 2mm groove surface modification is seen to have a significantly higher effect on the heat flux of the horizontal cylinder than the 3 mm grooves, smooth or knurled surfaces.

Figure 3.3 shows the corresponding convective heat transfer coefficients based on the superheating temperature $T_{\text{sur}} - T_{\infty}$. In our LN_2 pool-boiling measurements, surface geometry—rather than orientation—sets the scale of the heat-transfer coefficient. Using the smooth cylinder as a baseline, the **2 mm grooved** surface yields the greatest enhancement, with h higher by roughly $\sim 3.9\times$ at $\Delta T \approx 5$ K, tapering to $\sim 2.4\times$ by $\Delta T \approx 10$ K. The **3 mm grooved** surface is consistently second, about $\sim 2.8\times$ (at 5 K) down to $\sim 1.6\times$ (at 10 K) above smooth. The **knurled** surface shows a more modest but clear benefit, about $\sim 2.5\times$ (at 5 K) falling to $\sim 1.4\times$ (at 10 K). Thus, across the nucleate regime the ordering is *2 mm groove* > *3 mm groove* > *knurled* > *smooth*, with gaps widest at low superheat and narrowing as ΔT increases toward the high-flux end. Given the estimated uncertainties ($\approx \pm 20\%$ in q'' and ± 0.3 K in ΔT), these factors comfortably exceed experimental scatter and the ranking remains robust.

The current results can be compared to those of previous studies. For example, Sathyabhama [10] reported an increase in the rate of heat transfer with increasing groove depth and

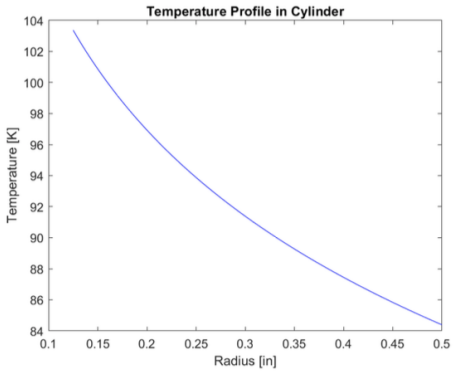

(a) Theoretical temperature profile through a test cylinder based on the thermocouple readings

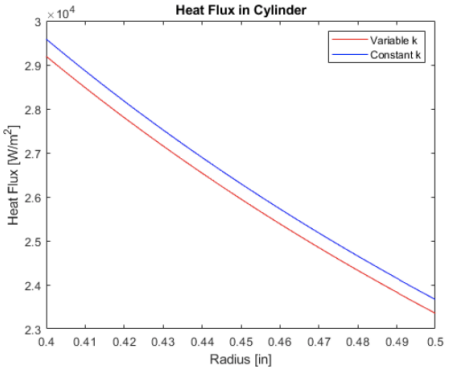

(b) Corrected heat flux throughout cylinder

Figure 3.1

decreasing channel width. They attributed the improved heat transfer to improved bubble dynamics due to the larger heat transfer area and other considerations. Grooves and channels were seen to enhance the heat flux by as much as 2-3 times [10], with Sathyabhama et al. [14] also showing significant increases with horizontal grooved cylinders. Microstructuring on cylinders was also studied by Hossain [15] and others, and was seen to have a benefit ranging from 60-80% [16] up to a factor of 2 [17], or up to a factor of 5 in the case of microchannels [18]. Surtaev [9] studied porous coatings and found a heat transfer enhancement of up to 300% using a technique of measuring power input and surface temperature to determine heat flux. This technique was impractical for this study due to the non-uniformities in the cartridge heaters employed.

3.1 Surface Area Correction

The results presented above did not explicitly address the increase in surface area for grooved cylinders. For the grooved cylinder, the convective heat transfer coefficient can be adjusted based on Eqs. (6) and (7), where the area ratio $\frac{A}{A_g} = 0.5205$ is based on the fin geometry. This correction suggests that the surface area-corrected heat transfer coefficients, h_g, are

shown in Fig. 9. Because the exposed area of the grooved cylinder is larger than that of the smooth cylinder, this would suggest a decrease in the actual heat transfer coefficient of about 50%.

$$Q = A \cdot h(T_{\text{sur}} - T_\infty) = A_g \cdot h_g(T_{\text{sur}} - T_\infty) \tag{6}$$

$$h_g = \frac{A}{A_g} h_s \tag{7}$$

3.2 Fin Efficiency Correction

A more complete accounting of the effects of grooves on the heat flux involves consideration of the actual grooved-surface geometry and heat transfer. The grooves effectively create a fin geometry, where the fins can be considered extensions on top of the underlying wall. The exposed area of each such fin, neglecting the tip regions, is given by

$$A_f = 2\pi(r_o^2 - r_i^2) \tag{8}$$

The corresponding exposed area between each pair of fins is then

$$A_b = 2\pi r_i t_b and \tag{9}$$

Taking the base temperature of the fin to be equal to the temperature of the surface between the fins gives for the total heat flow for each fin/base combination:

$$Q = h(T_b - T_\infty)\left[\eta A_f + A_b\right] \tag{10}$$

This formulation assumes that the heat transfer coefficient is constant over the fin/base region. Normalizing this heat flow by the corresponding heat flow in the absence of the fin, $Q_b = h(T_b - T_\infty)2\pi r_i(t_b + t_f)$, then gives

$$\frac{Q}{Q_b} = \frac{(\eta(r_o^2 - r_i^2) + r_i t_b)}{r_i(t_b + t_f)} \frac{h_f}{h} \tag{11}$$

where h_f is the equivalent heat transfer coefficient in the presence of fins based on the temperature difference $T_b - T_\infty$ and the baseline heat transfer coefficient, h.

The fin efficiency can be estimated using the formulation presented by Gardner [19], which takes into account the temperature decrease from the base region to the fin tip (heat transfer from the fin tip is neglected in this analysis). The efficiency has estimated values ranging from 0.6 to 0.9 for the geometry and baseline heat transfer coefficient of this investigation. With the estimated efficiency values, the corrected heat transfer coefficient can be calculated using the following equation for a given measured total heat flow:

$$\frac{h_f}{h} = \frac{r_i(t_b + t_f)}{\eta(r_o^2 - r_i^2 + r_o t_f) + r_i t_b} \tag{3.1}$$

However even with this correction, a substantial increase to heat flux is indicated due to surface modification. The amount of this increase rages from 4.5-13 for the horizontal cylinder.

3.3 Comparative performance with corrected measurements

Applying the variable-conductivity correction to the heat flux (2% lower) leaves the enhancement factors essentially unchanged relative to the nominal analysis. When we further express the grooved results on the *true* wetted area A_g (i.e., $h_g = Q/(A_g \Delta T)$) and include a fin-effectiveness factor η_f ($h_f = \eta_f h_g$), the apparent gains for the grooved cylinders are reduced in proportion to A_g/A and η_f, but the ordering remains robust across 3–10 K superheat: *2 mm groove* > *3 mm groove* > *knurled* > *smooth*. Quantitatively, the $k(T)$ correction changes all reported h values by 2% (within experimental scatter), while area and fin corrections reduce the grooved-cylinder multipliers by a geometry-dependent factor; the qualitative conclusions are unaffected.

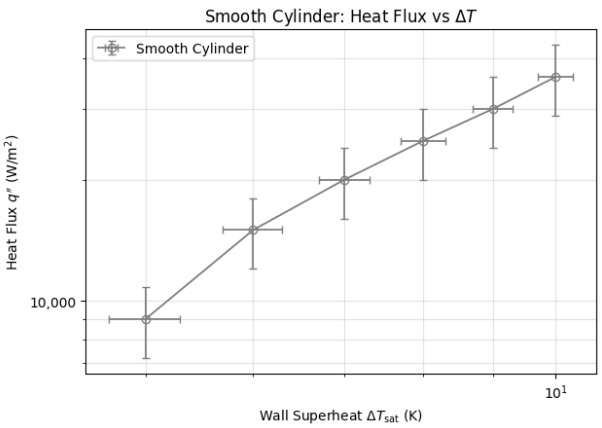

(a) Smooth cylinder

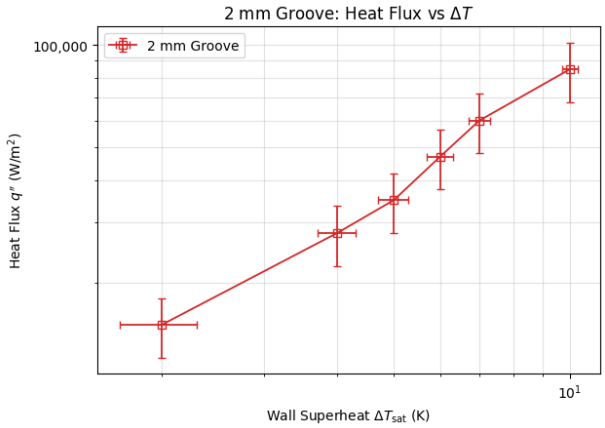

(b) 2 mm groove

Figure 3.2: Heat flux q'' vs. wall superheat ΔT for four surface geometries.

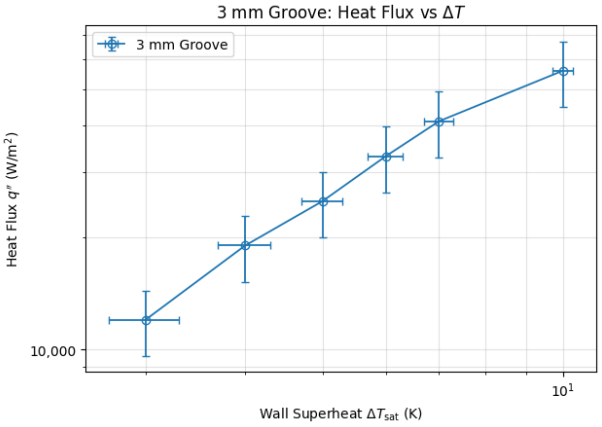

(c) 3 mm groove

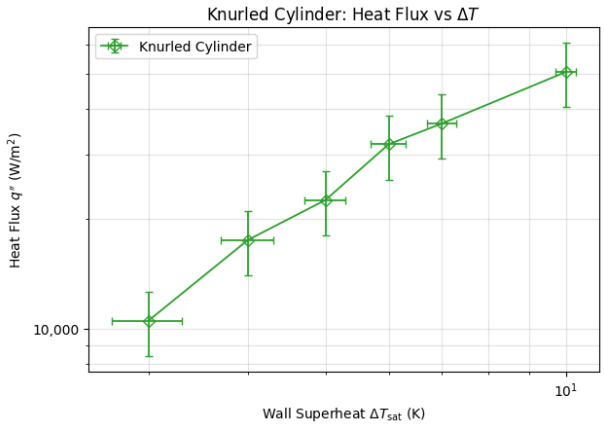

(d) Knurled cylinder

Figure 3.2: Heat flux q'' vs. wall superheat ΔT (continued).

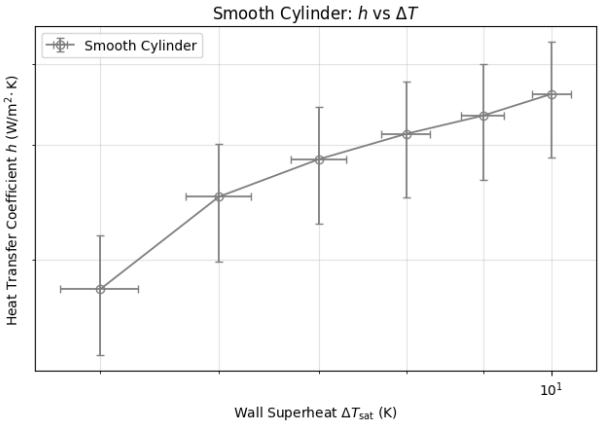

(a) Smooth cylinder

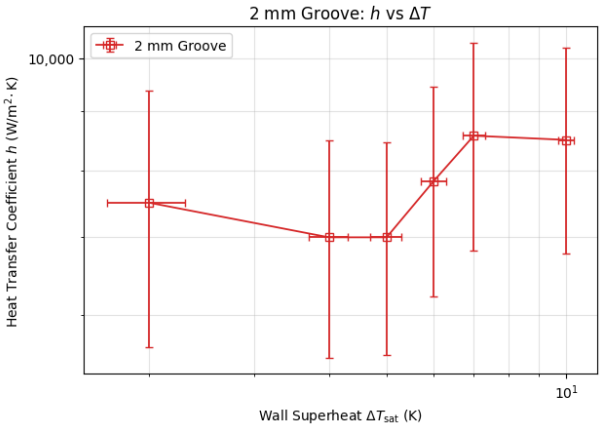

(b) 2 mm groove

Figure 3.3: Heat-transfer coefficient h vs. wall superheat ΔT for four surface geometries.

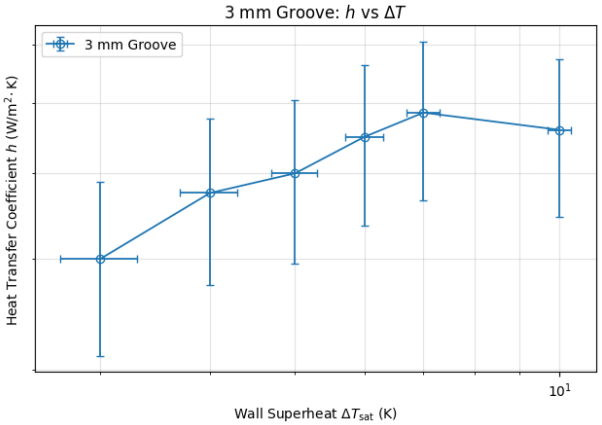

(c) 3 mm groove

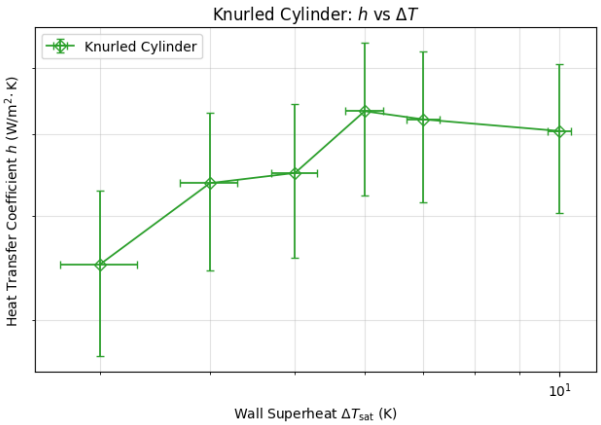

(d) Knurled cylinder

Figure 3.3: Heat-transfer coefficient h vs. wall superheat ΔT (continued).

Chapter 4

IMAGING

Close-up visualization of cryogenic boiling was pursued first with a submerged GoPro and then with a purged endoscope. The new custom cryogenic dewar includes optical windows and will enable two-axis, external high-speed imaging; the UW's Phantom v1211 can exceed 100000 fps, sufficient for expected bubble departure rates [3]. The dewar's nominal volume is 12.9 L and its inside diameter is approximately 18.9 cm. [8].

In submerged GoPro trials, images routinely fogged due to condensation and icing on the housing. We therefore adopted a purged-endoscope approach with the battery external to the bath and a continuous helium purge across the lens. This configuration reduced fogging and allowed preliminary size estimates of nucleate bubbles. Using the in-frame ruler for scale, the endoscope outer diameter was measured at $\approx 16 \pm 2$ mm, and observed bubble diameters were on the order of 2 mm, consistent with the expected critical bubble size for LN_2 at 1 atm.

Practical issues encountered included: compact housing geometry, susceptibility to leaks

Figure 4.1: Bubbles arising from the smooth cylinder

and burst seals, long cryo-epoxy cure times, purge flow rates that exhausted helium quickly, pressure-gauge replacement, and mechanical damage to polycarbonate feedthroughs during drilling. Even so, the purged endoscope provided the most usable images to date; the clearest imagery was obtained over the smooth cylinder. With the arrival of the optical-access dewar, future work will transition to external high-speed imaging to quantify bubble sizes, site density, and departure frequencies with minimal fogging [3].

Chapter 5

CONCLUSIONS

Experiments were conducted using liquid nitrogen to assess the impact of surface modifications on the rates of heat transfer and boiling in the nucleate boiling regime at one atmosphere pressure. Tests were done in both the horizontal and vertical orientations with both smooth and a grooved cylinders. Variations in the thermal conductivity were taken into account using the NIST database and averaging the results to get an effective thermal resistance within the cylinders. The grooved surfaces were shown to provide an increase in the heat transfer coefficient, with a larger increase for the horizontal case (about an order of magnitude compared to a factor of two for the vertical case). Correcting for the change in surface area alone suggested that the heat transfer coefficients were somewhat lower than the measured values for the grooved cylinders. With this correction applied, the increase in the rate of heat transfer due to surface modification amounted to a factor of as much as 13 for the horizontal cylinder. For the vertical cylinder, the computed heat transfer increased by up to a factor of 1.4 for the upper position, but was less for the lower position. However, a more complete analysis considering the fin effectiveness of the grooved cylinders suggests that the heat transfer coefficients were somewhat higher (approximately 12-15% greater than baseline measurements) for the grooved cylinders. This study also found a higher heat transfer coefficient for the middle of the cylinder compared to lower down in the vertical case, while no axial difference was found in the horizontal case. Future work on this topic will include more complicated groove structures, different material variations and looking at different geometries other than cylinders. Imaging progressed from a submerged GoPro (limited by fogging and housing reliability) to an externally purged endoscope that consistently yielded clear views of nucleate boiling on the 2.5 cm OD cylinder. Using cylinder markings as a

fiducial, bubble diameters were ≈2 mm, consistent with expectations for LN_2 at 1 atm and the surface geometries tested. Although the present frame rates prevented estimation of bubble departure velocity, the newly acquired two-viewport cryogenic dewar and planned Phantom high-speed camera will enable quantitative bubble-dynamics measurements (size, frequency, velocity) in future work.

BIBLIOGRAPHY

[1] J. L. Yanosy. Cryogenics and ECLSS–past, present, and future challenges. *SAE Transactions*, pages 469–477, 2000.

[2] N Sack V Drach and J Fricke. Transient heat transfer from surfaces of defined roughness into liquid nitrogen. *International journal of heat and mass transfer*, 39(9):1953–1961, 1996.

[3] Xiaobin Zhang et al. Visualization study of nucleate pool boiling of liquid nitrogen with quasi-steady heat input. *Cryogenics*, 72:14–21, 2015.

[4] J. S. Mehta and S. G. Kandlikar. Heat transfer enhancement during pool boiling of water over horizontal and vertical tubes with micro structured surfaces. *International Conference on Nanochannels, Microchannels, and Minichannels*, 44793:71–80, 2012.

[5] M. et al., Mercado. Assessment of two-phase heat transfer coefficient and critical heat flux correlations for cryogenic flow boiling in pipe heating experiments. *International Journal of Heat and Mass Transfer*, 133:295–315, 2019.

[6] Jason Hartwig, Samuel Darr, and Anthony Asencio. Assessment of existing two phase heat transfer coefficient and critical heat flux correlations for cryogenic flow boiling in pipe quenching experiments. *International Journal of Heat and Mass Transfer*, 93 (441–463), 2016.

[7] C. Bombardieri and C. Manfletti. Influence of wall material on nucleate pool boiling of liquid nitrogen. *International Journal of Heat and Mass Transfer*, 94:1–8, 2016.

[8] R. Moore and J. Hermanson. Evaluating the complete pool boiling curve for liquid nitro-

gen. *Final Report, NASA Grant and Cooperative Agreement Number 80NSSC19K1630*, 2022.

[9] A. S. Surtaev et al. Heat transfer and crisis phenomena at pool boiling of liquid nitrogen on the surfaces with capillary-porous coatings. *International Journal of Heat and Mass Transfer*, 108:146–155, 2017.

[10] A. Sathyabhama. Nucleate pool boiling heat transfer from a flat-plate grooved surface. *Journal of Enhanced Heat Transfer*, 22(3), 2015.

[11] I. Gogonin. Influence of the thickness of a wall and of its thermophysical characteristics on the critical heat flux in boiling. *Journal of Engineering Physics Thermophysics*, 82 (6), 2009.

[12] Le J. Marquardt, E. and R Radebaugh. Cryogenic material properties database. *Cryocoolers 11*, pages 681–687, 2002.

[13] Theodore L. Bergman et al. *Introduction to heat transfer*. John Wiley Sons, 2011.

[14] A. Sathyabhama and S. Prashanth. Experimental investigation on boiling heat transfer coefficient enhancement using grooves for cooling of electronic devices. *Fourteenth Intersociety Conference on Thermal and Thermomechanical Phenomena in Electronic Systems (ITherm)*, pages 466–472, 2014.

[15] Md. Rakib Hossain, Md. Imran Hossain Talukder, and Md. Ashiqur Rahman. Study of pool boiling on flat and micro-grooved brass and copper surfaces. *AIP Conference Proceedings*, 2121(1):030012, 2019.

[16] Balkrushna A. Shah et al. Experimental investigation of nucleate boiling over a smooth and micro-grooved cylindrical surface. *Technologies for Sustainable Development*, pages 323–328., 2020.

[17] Houli Liu et al. Enhancement of pool boiling heat transfer using 3d-printed groove structure. *International Journal of Heat and Mass Transfer*, 183:122155, 2022.

[18] R. Kumar and B. Premachandran. Enhancement of pool boiling performance through an asymmetric dual v-groove microchannel structured surface. *Available at SSRN 4584051*, 2023.

[19] K. A. Gardner. Efficiency of extended surface. *Transactions of the American Society of Mechanical Engineers*, 67(8):621—-628, 1945.

[20] M Shiotsu A Sakurai and K Hata. A general correlation for pool film boiling heat transfer from a horizontal cylinder to subcooled liquid: Part 2—experimental data for various liquids and its correlation. *Journal of Heat Transfer*, 112:441—-450, 1990.

[21] N. R. Mikhail. Studies in heat transfer to boiling liquids at low temperatures. *Ph.D. thesis*, 1952.

[22] D. N. Lyon. Peak nucleate-boiling heat fluxes and nucleate-boiling heat-transfer coefficients for liquid n2, liquid o2 and their mixtures in pool boiling at atmospheric pressure. *International Journal of Heat and Mass Transfer*, 7(10):1097—-1116, 1964.

[23] Peters J. Haselden, G. et al. Heat transfer to boiling liquid oxygen and liquid nitrogen. *Trans Inst Chem Eng*, 27:201—-208, 1949.

[24] V. Grigoriev et al. Concerning the influence of thermal properties of heating surface material on heat transfer intensity of nucleate pool boiling of liquids including cryogenic ones. *Cryogenics*, 17(2):94—-96, 1977.

[25] E. L. Park Jr. Nucleate and film boiling heat transfer to methane and nitrogen from atmospheric pressure to the critical pressure. 1965.

[26] Xiaobin Zhang et al. Cfd simulations and experimental verification on nucleate pool boiling of liquid nitrogen. *Physics Procedia*, 67:569—-575, 2015.

[27] J. Thome and W. Bald. Nucleate pool boiling in cryogenic binary mixtures. *Proceedings of the 7th International Cryogenic Engineering Conference, London, S*, pages 523—-530, 1978.

[28] D. Labountzov. Generalized correlation for nucleate boiling. *Teploenergetika*, 7(5): 76—-80, 1960.

[29] M. McNelly. A correlation of rates of heat transfer to nucleate boiling of liquids. *A correlation of rates of heat transfer to nucleate boiling of liquids*, 7:18—-34, 1953.

[30] K. Stephan and M. Abdelsalam. Heat-transfer correlations for natural convection boiling. *International Journal of Heat and Mass Transfer*, 23(1):73—87, 1980.

[31] W. M. Rohsenow. A method of correlating heat-transfer data for surface boiling of liquids. *Transactions of the American Society of Mechanical Engineers*, 74(6):969—-975, 1952.

[32] M. Cooper. "heat flow rates in saturated nucleate pool boiling-a wide-ranging examination using reduced properties. *Advances in heat transfer*, 16:157—-239, 1984.

[33] V.and others Borishansky. Heat transfer during nucleate boiling of water and ethyl alcohol, in a volume of collection of articles. *Aspects of heat transfer and hydraulics of two-phase mixtures*, pages 75–93, 1961.

[34] C. B. Johler. A study of the nucleate boiling of liquid nitrogen, liquid argon, and liquid carbon monoxide from atmospheric to near the critical pressure. *Master's thesis*, 1969.

[35] C. Cobb. A study of surface and geometric effects on the nucleate boiling of liquid nitrogen and liquid argon from atmospheric to the critical pressure. *Ph.D. thesis*, 1967.

[36] S.S. Kutateladze. On the transition to film boiling under natural convection. *Kotloturbostroenie*, 3:10, 1948.

[37] S. S Kutateladze. *Heat transfer in condensation and boiling*, 3770, 1959.

[38] H. Forster and N. Zuber. Dynamics of vapor bubbles and boiling heat transfer. *AIChE Journal*, 1(4):531—-535, 1955.

[39] D. Gorenflo and D. Kenning. H2 pool boiling. *VDI heat atlas*, pages 757—-792, 2009.